Applied Physics Express

LETTERS

High-speed and highly efficient Si optical modulator with strained SiGe layer

Applied Physics Express **11**, 032201 (2018)
https://doi.org/**10.7567/APEX.11.032201**

High-speed and highly efficient Si optical modulator with strained SiGe layer

Junichi Fujikata[1]*, Masataka Noguchi[1], Younghyun Kim[2], Jaehoon Han[2], Shigeki Takahashi[1], Takahiro Nakamura[1], and Mitsuru Takenaka[2]

[1]*Photonics Electronics Technology Research Association (PETRA), Tsukuba, Ibaraki 305-8569, Japan*
[2]*The University of Tokyo, Bunkyo, Tokyo 113-8656, Japan*

*E-mail: j-fujikata@petra-jp.org

Received January 11, 2018; accepted January 18, 2018; published online February 5, 2018

We developed a high-speed and highly efficient depletion-type Si optical modulator (Si-MOD) with a pn junction by applying a p-type-doped strained SiGe layer, which was stacked on a lateral pn junction-type Si-MOD. We designed an optimum Si-MOD, which is one of the most efficient Si-MODs with a pn junction, and demonstrated highly efficient modulations of 0.67 and 0.81 V·cm for $V_\pi L$ at dc reverse bias voltages of −0.5 and −2 V_{dc}, respectively. We also demonstrated a high-speed operation of 25 Gbps for the Si-MOD at a wavelength of around 1.3 μm.

Silicon photonics is a highly active field of research because it offers low cost, low power consumption, and large bandwidth for optoelectronic solutions for applications ranging from telecommunications to chip-to-chip interconnects.[1)] To realize an effective photonics-electronics convergence system, it is very important to achieve a high-speed and highly efficient silicon optical modulator (Si-MOD).[2–14)]

Among the various Si-MODs demonstrated so far, Mach–Zehnder Si-MODs based on the free carrier plasma dispersion effect have been mostly reported for high-speed modulation and broad-wavelength operation.[5–11)] However, carrier-depletion Si modulators need a relatively long phase shifter or a high driving voltage because of the weak plasma dispersion effect in Si,[15)] making them unfavorable for large-scale integration. It has been reported that travelling wave electrodes (TWEs) are designed to match the 50 Ω impedance for a high-speed operation of around 30 GHz.[16,17)] However, these structures result in a low power efficiency because of the attenuation of the driving electric power in them. Therefore, segmented lumped electrodes have been proposed to improve the power efficiency.[18)] However, there is a trade-off between modulation efficiency and frequency response.

To overcome such trade-off, it has been proposed that Si MODs with a strained SiGe layer enhance the free carrier plasma dispersion effect by reducing the effective mass of holes in SiGe because the effect is inversely proportional to the effective carrier mass.[19,20)] The enhancement of the carrier plasma dispersion effect using a strained SiGe layer is expected to improve the power efficiency because it contributes to a lower capacitance with a sufficient modulation efficiency. In Ref. 21, a high modulation efficiency of 0.81 V·cm and 25 Gbps operation have been reported to be achieved by applying a p-type SiGe layer to a Si optical modulator. In Ref. 22, the application of an in situ boron-doped p-type SiGe layer has been reported to be effective in achieving a high-performance Si-MOD. However, the optimum thickness of the p-type strained SiGe layer has not been investigated analytically.

In this study, we design an optimum Si-MOD by applying a p-type-doped strained SiGe layer on the Si pn junction of a rib waveguide and analyze the enhancement factor for the p-type-strained SiGe layer on the Si pn junction. We report highly efficient modulations of 0.67 and 0.81 V·cm at −0.5 and −2 V_{dc}, respectively, which are one of the most efficient modulations in Si-MODs with a pn junction. We also evaluate the frequency response and demonstrate a high-speed and highly efficient operation at 25 Gbps for the Si-MOD with the p-type-doped strained SiGe layer at a wavelength of around 1.3 μm.

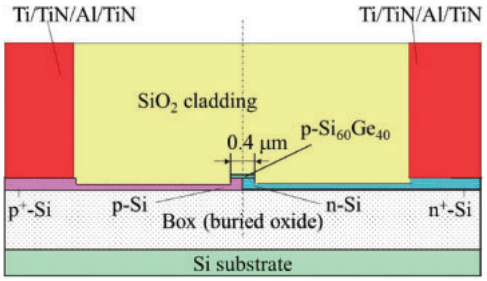

Fig. 1. Schematic diagram of depletion-type Si-MOD with strained SiGe layer.

Figure 1 shows a schematic cross section of a depletion-type Si-MOD with a strained SiGe layer. The Si-MOD consists of an asymmetric Mach–Zehnder interferometer (MZI), in which the difference in Si waveguide (Si-WG) length was 20 μm. The fabrication process started with 4 inch silicon-on-insulator (SOI) wafers with an SOI thickness of 180 nm for a wavelength of 1.3 μm. After the ion implantation of boron and phosphorus, Si-WGs were patterned by electron beam lithography and dry etching. After SiO_2 layer deposition, SiGe-selective-growth windows were formed on the phase shifter of the Si rib waveguide with a lateral pn junction. Then, a 40-nm-thick strained SiGe layer was selectively grown by reduced-pressure chemical vapor deposition (RP-CVD) from the mixed gas source of SiH_4 and GeH_4. Next, boron ions were implanted into the SiGe layer and activated at 700 °C. Finally, the upper cladding layer and contact hole were formed, and the stacked electrodes of the Ti/TiN/Al layers were deposited and patterned. The doping densities of p-Si, n-Si, and p-SiGe were 1.0×10^{18}/cm^3. In the experiment, the phase shifter length was 500 μm. The structural design of the Si-MOD with a p-type-doped strained SiGe layer was performed by the linked simulation of carrier transport and optical mode analyses.

Figure 2(a) shows a transmission electron microscopy (TEM) image of the SiGe/Si interface, and Fig. 2(b) shows the measured Raman spectra for a 1 mm^2 pattern of a SiGe layer on Si and a selectively grown SiGe layer on a 400-nm-

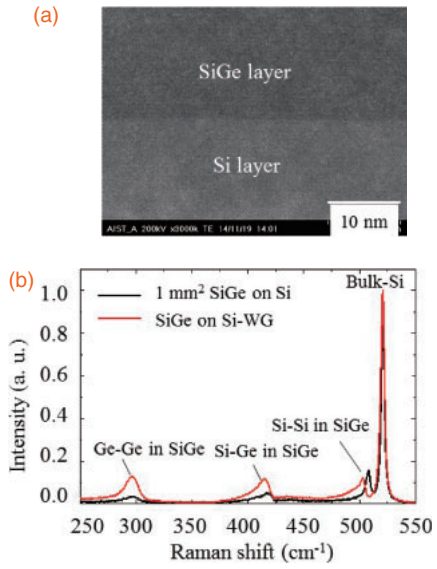

Fig. 2. (a) TEM image of SiGe/Si layers and (b) measured Raman spectra for 1 mm^2 SiGe on Si and selectively grown SiGe on Si-WG.[21)]

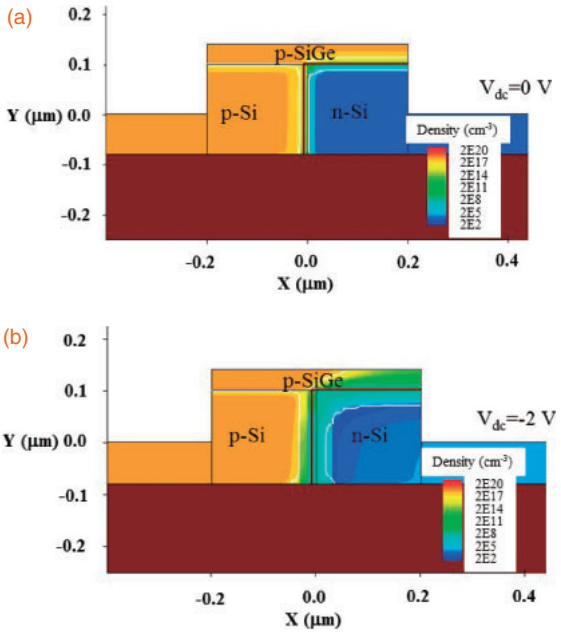

Fig. 3. Contour maps of free carrier density for (a) 0 and (b) $-2\,V_{dc}$.

wide Si-WG. From the TEM image, crystalline defects were barely observed at the interface between the SiGe and Si layers in the case of the selective growth of the SiGe layer on the Si-WG. By Raman spectral analysis, the Ge composition of SiGe was estimated to be around 40%.[23)]

The crystalline strain of a SiGe layer was estimated to be 1.8% on the 1 mm^2 pattern, which is comparable to the theoretical value. On the other hand, it was estimated to be 1.5% for the selective growth of SiGe on the Si-WG with a lateral pn junction. Therefore, the biaxial strain of SiGe was slightly relaxed because the selective growth of the SiGe pattern had a high aspect ratio with a 400 nm width and a 500 μm length, and this uniaxial dimension contributed to the small relaxation of the biaxial strain.

Figure 3 shows contour maps of free carrier density for the Si-MOD with a p-type strained SiGe layer in the cases of (a) 0 and (b) $-2\,V_{dc}$ obtained by simulation. With a reverse bias voltage of $-2\,V_{dc}$, the depletion layer thickness at the interface of a Si-based lateral pn junction and a p-type SiGe and n-type Si heterojunction increases, which results in a higher optical modulation efficiency because the overlap between an optical mode field and a carrier density modulation region increases. In this study, the depletion of the p-type strained SiGe layer compared with that of p-type Si is also expected to contribute to the large enhancement of optical modulation efficiency.

The well-known formulas for optical refractive index change and absorption due to free electrons and holes are as follows:[15)]

$$\Delta n = -\frac{e^2\lambda^2}{8\pi^2c^2\varepsilon_0 n}\left(\frac{\Delta N_e}{m^*_{ce}} + \frac{\Delta N_h}{m^*_{ch}}\right), \quad (1)$$

$$\Delta\alpha = \frac{e^3\lambda^2}{4\pi^2c^3\varepsilon_0 n}\left(\frac{\Delta N_e}{m^{*2}_{ce}\mu_e} + \frac{\Delta N_h}{m^{*2}_{ch}\mu_h}\right). \quad (2)$$

From the formulas, the optical refractive index change effect is determined to be inversely proportional to the effective carrier mass. Therefore, $V_\pi L$ is expected to be enhanced by using a p-type strained SiGe layer, which has a lower effective hole mass with an increase in Ge composition than Si.[24)]

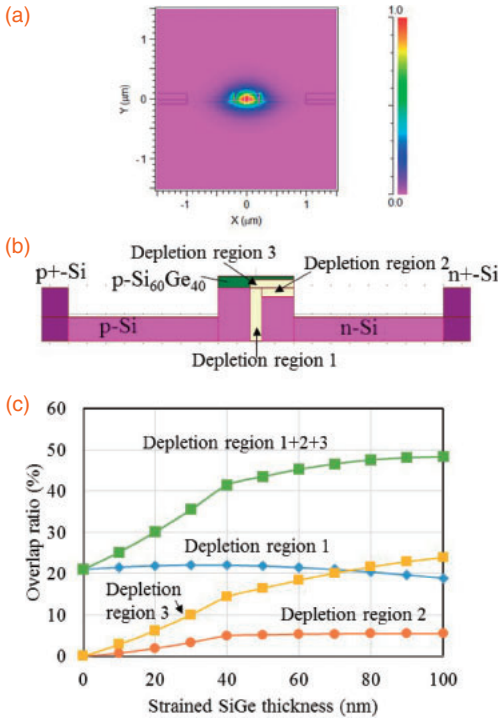

Fig. 4. (a) Simulation results of electric field intensity contour map of optical mode field in cross section of Si optical modulator with 40-nm-thick strained $Si_{60}Ge_{40}$ layer, (b) schematic diagram of depletion region definitions, and (c) dependence of overlap ratio between optical mode field and depletion regions for Si optical modulator with strained $Si_{60}Ge_{40}$ layer.

Figures 4(a) and 4(b) show the simulation results of the electric field intensity contour map of the optical mode field in the cross section of a Si optical modulator with a 40-nm-thick strained $Si_{60}Ge_{40}$ layer and a schematic diagram of depletion region definitions, respectively. Depletion region 1 is defined to be that of a lateral pn junction, depletion region 2 is that of n-type Si at the heterojunction of n-type Si and p-type $Si_{60}Ge_{40}$, and depletion region 3 is that of a p-type strained $Si_{60}Ge_{40}$ layer at the heterojunction. The depletion

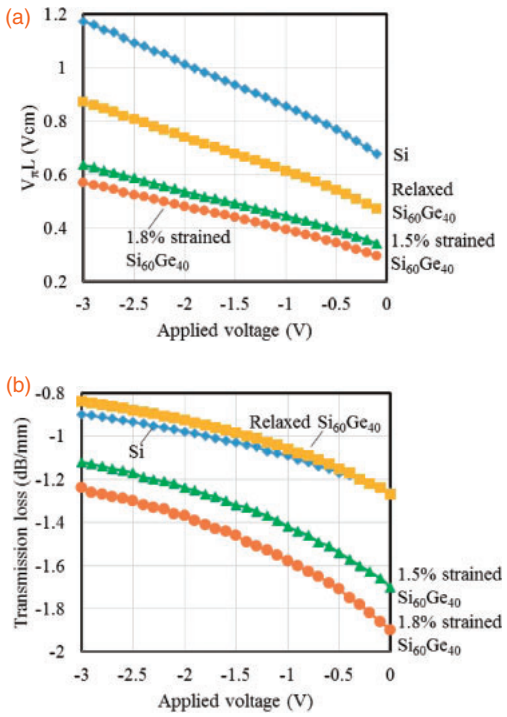

Fig. 5. Simulation results of dependences of (a) $V_\pi L$ and (b) propagation loss on applied voltage for Si-MOD with p-type-doped Si and strained and unstrained $Si_{60}Ge_{40}$ layers.

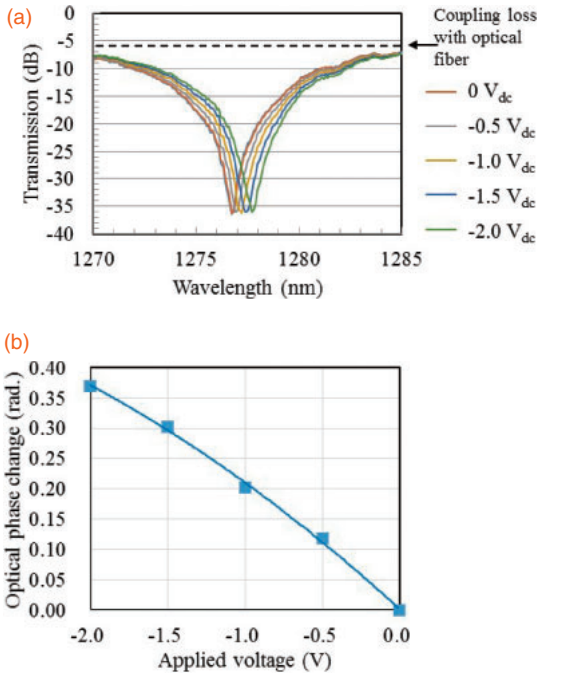

Fig. 6. (a) Transmission spectra of Si-MOD with strained SiGe layer dependence on applied reverse bias voltage and (b) optical phase change dependence on V_{dc}.

regions were simulated using technology computer-aided design (TCAD). In the simulation, the refractive index was set to be 3.50 for Si and 3.84 for $Si_{60}Ge_{40}$.

Figure 4(c) shows the calculated overlap ratio between an optical mode field and depletion regions for Si and strained $Si_{60}Ge_{40}$ layers as a parameter of strained $Si_{60}Ge_{40}$ layer thickness. In the calculation, the overlap ratio for a strained $Si_{60}Ge_{40}$ depletion layer was defined to be 2.2 times higher than the actual overlap ratio to analyze the contribution of the free carrier dispersion effect of a strained $Si_{60}Ge_{40}$ layer to optical phase modulation. That is, the free carrier dispersion effect is estimated to be 2.2 times larger for a strained $Si_{60}Ge_{40}$ layer than for a Si layer in the case of the same overlap ratio because of the 2.2 times lighter effective hole mass for a strained $Si_{60}Ge_{40}$ layer.[24] As the strained $Si_{60}Ge_{40}$ layer thickness increases to up to 40 nm, the overlap ratio increases monotonically to about 40%. In this case, an approximately 15% overlap ratio can be obtained for depletion region 3, which contributes to an optical overlap ratio that is about twice as high as that in the case of a 40-nm-thick strained $Si_{60}Ge_{40}$ layer on the lateral pn junction of the Si modulator compared with that of the lateral pn junction-type Si modulator with only depletion region 1. The overlap ratio increases gradually for strained $Si_{60}Ge_{40}$ layers that are more than 40 nm thick. However, the nondepleted region of a strained $Si_{60}Ge_{40}$ layer results in the enhancement of the free carrier absorption effect. Therefore, a 40-nm-thick strained $Si_{60}Ge_{40}$ layer is effective for realizing a high modulation efficiency and a low optical loss.

Figures 5(a) and 5(b) respectively show the simulation results of the dependences of $V_\pi L$ and optical loss on V_{dc} for the Si-MOD with 40-nm-thick p-type-doped Si and p-type-doped strained $Si_{60}Ge_{40}$ layers with 1.5 and 1.8% compressive strains. In the simulation, effective hole mass was estimated from the report indicating that it is inversely proportional to strain,[25] and hole carrier mobility was estimated from the report indicating that it is proportional to stress, that is, strain.[26] By applying the strained $Si_{60}Ge_{40}$ layer, approximately twice the optical modulation efficiency of $V_\pi L$ can be obtained. In the case of a relaxed $Si_{60}Ge_{40}$ layer, the enhancement factor of $V_\pi L$ decreases to about 50%, but optical loss is comparable to that in the case of a p-type-doped Si layer. This is because the enhancement factor of hole mobility is smaller than the reduction in effective hole mass in the case of a strained SiGe layer.[24]

Next, we studied the modulation efficiency and high-speed characteristics of the fabricated Si-MOD with a strained SiGe layer at a wavelength of 1.3 μm. Figures 6(a) and 6(b) show the transmission spectra of the Si-MOD with a strained SiGe layer dependence on V_{dc} and an optical phase change dependence on V_{dc}, respectively. The spectrum shifted to a longer wavelength, and the spectral dip wavelength changed almost linearly with an increase in V_{dc}. The estimated modulation efficiency was 0.81 V·cm at -2 V_{dc}, which is one of the most efficient values among depletion-type Si-MODs with a pn junction. At V_{dc} of around -0.5, 0.67 V·cm was also obtained because the depletion of a p-type strained SiGe layer is more effective at low V_{dc} values.

Figure 7 shows the (a) 3 dB bandwidth and capacitance of the pn junction dependence on V_{dc} and (b) the frequency response for a SiGe optical modulator with a 500-μm-long phase shifter at -2 V_{dc}. At lower reverse biases of around -0.5 V_{dc}, the depletion thickness is relatively small, and the 3 dB bandwidth is smaller because of the higher capacitance of the pn junction. For reverse bias voltages higher than -1 V_{dc}, the bandwidth almost saturated at around 12 GHz, which is comparable to that of a Si modulator without a strained SiGe layer. This means that a strained p-type-SiGe

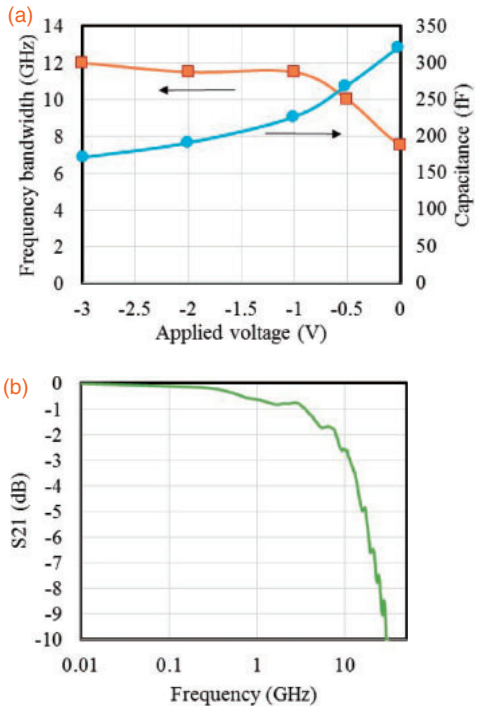

Fig. 7. (a) 3 dB bandwidth and capacitance of pn junction dependence on V_{dc} and (b) frequency response for a SiGe optical modulator with a 500-μm-long phase shifter at $-2\,V_{dc}$.

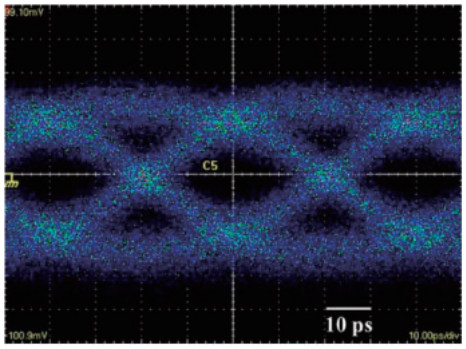

Fig. 8. Measured eye diagram at 25 Gbps with $2^{31}-1$ PRBS at wavelength of approximately 1.3 μm at 2.5 V_{pp} and $-2\,V_{dc}$.

layer at the heterogeneous p-SiGe/n-Si junction is almost fully depleted at a higher V_{dc}, as shown in Fig. 5, which decreases the capacitance at pn junctions, accompanied by a slight increase in series resistance.

Figure 8 shows the measured eye diagram at 25 Gbps with a $2^{31}-1$ pseudo-random binary sequence (PRBS) when V_{dc} was -2 V and the differential RF drive voltage was 2.5 V_{pp}. In this experiment, modulation operation was selected to be at a -3 dB balance point in the asymmetric MZI by tuning the input light wavelength to approximately 1.3 μm. The extinction ratio (ER) was about 3 dB, and the insertion optical loss was estimated to range from 1.5 to 2.0 dB, which will be improved by optimizing the SiGe composition and strain to decrease the optical absorption by bandgap shrinkage.[22,27]

Acknowledgment This study is based on the results obtained from a project commissioned by the New Energy and Industrial Technology Development Organization (NEDO).

1) G. T. Reed, G. Mashanovich, F. Y. Gardes, and D. J. Thomson, Nat. Photonics **4**, 518 (2010).
2) Q. Xu, B. Schmidt, S. Pradhan, and M. Lipson, Nature **435**, 325 (2005).
3) Y. H. Kuo, Y. K. Lee, Y. Ge, S. Ren, J. E. Roth, T. I. Kamins, D. A. B. Miller, and J. S. Harris, Nature **437**, 1334 (2005).
4) J. Liu, M. Beals, A. Pomerene, S. Bernardis, R. Sun, J. Cheng, L. C. Kimerling, and J. Michel, Nat. Photonics **2**, 433 (2008).
5) W. M. J. Green, M. J. Rooks, L. Sekaric, and Y. A. Vlasof, Opt. Express **15**, 17106 (2007).
6) L. Liao, A. Liu, D. Rubin, J. Basak, Y. Chetrit, H. Nguyen, R. Cohen, N. Izhaky, and M. Paniccia, Electron. Lett. **43**, 1196 (2007).
7) F. Y. Gardes, D. J. Thomson, N. G. Emerson, and G. T. Reed, Opt. Express **19**, 11804 (2011).
8) D. J. Thomson, F. Y. Gardes, J. M. Fedeli, S. Zlatanovic, Y. F. Hu, B. P. P. Kuo, E. Myslivets, N. Alic, S. Radic, G. Z. Mashanovich, and G. T. Reed, IEEE Photonics Technol. Lett. **24**, 234 (2012).
9) D. M. Gill, J. E. Proesel, C. Xiong, J. S. Orcutt, J. C. Rosenberg, M. H. Khater, T. Barwics, S. Assefa, S. M. Shank, C. Reinholm, J. Ellis-Monaghan, E. Kiewra, S. Kamlapurkar, C. M. Breslin, W. M. J. Green, W. Haensch, and Y. A. Vlasof, IEEE J. Sel. Top. Quantum Electron. **21**, 3400311 (2015).
10) D. Patel, S. Ghosh, M. Chagnon, A. Samani, V. Veerasubramanian, M. Osman, and D. V. Plant, Opt. Express **23**, 14263 (2015).
11) M. Liu, X. Yin, E. Ulin-Avila, B. Geng, T. Zentgraf, L. Ju, F. Wang, and X. Zhang, Nature **474**, 64 (2011).
12) M. Liu, X. Yin, and X. Zhang, Nano Lett. **12**, 1482 (2012).
13) A. V. Krishnamoorthy, X. Zheng, D. Feng, J. Lexau, J. F. Buckwalter, H. D. Thacker, F. Liu, Y. Luo, E. Chang, P. Amberg, I. Shubin, S. S. Djordjevic, J. H. Lee, S. Lin, H. Liang, A. Abed, R. Shafiiha, K. Raj, R. Ho, M. Asghari, and J. E. Cunningham, Opt. Express **22**, 12289 (2014).
14) J. Fujikata, S. Takahashi, M. Takahashi, M. Noguchi, T. Nakamura, and Y. Arakawa, Jpn. J. Appl. Phys. **55**, 04EC01 (2016).
15) R. Soref and B. R. Bennett, IEEE J. Quantum Electron. **23**, 123 (1987).
16) M. Streshinsky, R. Ding, Y. Liu, A. Novack, Y. Yang, Y. Ma, X. Tu, E. K. S. Chee, A. E.-J. Lim, P. G.-Q. Lo, T. Baehr-Jones, and M. Hochberg, Opt. Express **21**, 30350 (2013).
17) Y. Yang, Q. Fang, M. Yu, X. Tu, R. Rusli, and G.-Q. Lo, Opt. Express **22**, 29978 (2014).
18) K. Yashiki, Y. Suzuki, Y. Hagihara, M. Kurihara, M. Tokushima, J. Fujikata, A. Ukita, K. Takemura, T. Shimizu, D. Okamoto, J. Ushida, S. Takahashi, T. Uemura, M. Okano, J. Tsuchida, T. Nedachi, M. Fushimi, I. Ogura, J. Inasaka, and K. Kurata, Proc. OFC2015, 2015, Th1G.1.
19) M. Takenaka and S. Takagi, IEEE J. Quantum Electron. **48**, 8 (2012).
20) Y. Kim, J. Fujikata, S. Takahashi, M. Takenaka, and S. Takagi, Opt. Express **24**, 1979 (2016).
21) J. Fujikata, M. Noguchi, Y. Kim, S. Takahashi, T. Nakamura, and M. Takenaka, 12th GFP2015, 2015, WD2.
22) J. Fujikata, M. Noguchi, J. Han, S. Takahashi, M. Takenaka, and T. Nakamura, 42nd ECOC2016, 2016, Tu.3.A.4.
23) F. Pezzoli, E. Bonera, E. Grilli, M. Guzzi, S. Sanguinetti, D. Chrastina, G. Isella, H. von Kanel, E. Wintersberger, J. Stangl, and G. Bauer, Mater. Sci. Semicond. Process. **11**, 279 (2008).
24) T. Manku, J. M. McGregor, A. Nathan, D. J. Roulston, J.-P. Noel, and D. C. Houghton, IEEE Trans. Electron Devices **40**, 1990 (1993).
25) J.-L. Ma, H.-M. Zhang, X.-Y. Wang, Q. Wei, G.-Y. Wang, and X.-B. Xu, J. Comput. Electron. **10**, 388 (2011).
26) L. Gomez, C. N. Chlairigh, P. Hashemi, and J. L. Hoyt, IEEE Electron Device Lett. **31**, 782 (2010).
27) D. V. Lang, R. People, J. C. Bean, and A. M. Sergent, Appl. Phys. Lett. **47**, 1333 (1985).